The ultrastructural organization of endoplasmic reticulum-plasma membrane contacts is conserved in epithelial cells

Authors:

Gary Hong Chun Chung[1], Maëlle Lorvellec[1,2], Paul Gissen[1,2], Franck Pichaud[1], Jemima J. Burden[1] and Christopher J. Stefan[1]

Affiliations:

[1] MRC Laboratory for Molecular Cell Biology, University College London, Gower Street, London WC1E 6BT, UK

[2] NIHR Great Ormond Street Hospital Biomedical Research Centre, University College London, Ormond Street, London, WC1N 1EH, UK

Correspondence: Jemima J. Burden, j.burden@ucl.ac.uk, ORCID 0000-0001-5894-7043
Christopher J. Stefan, c.stefan@ucl.ac.uk, ORCID 0000-0002-4118-5721

Running head: Conserved ER-PM contacts in epithelial cells

Summary: Quantitative electron microscopy of hepatocytes and epithelial spheroids reveals an extensive network of intra-cellular contacts between the endoplasmic reticulum and plasma membrane (ER-PM contacts) at lateral PM domains that form inter-cellular junctions, pointing out conserved roles of ER-PM contacts in epithelial cell and tissue architecture.

Keywords: apical domain, basal domain, bile canaliculi, cell-cell junctions, endoplasmic reticulum-plasma membrane contacts, epithelial cells, hepatocytes, lateral domain, oxysterol-binding protein related proteins

Abstract

Contacts between the endoplasmic reticulum and plasma membrane (ER-PM contacts) have important roles in membrane lipid and calcium dynamics. Yet, their organization in polarized epithelial cells has not been thoroughly described. Here, we examine ER-PM contacts in hepatocytes in mouse liver using electron microscopy, providing the first comprehensive ultrastructural study of ER-PM contacts in a mammalian epithelial tissue. Our quantitative analyses reveal strikingly distinct ER-PM contact architectures spatially linked to apical, lateral, and basal PM domains. Notably, we find that an extensive network of ER-PM contacts exists at lateral PM domains that form inter-cellular junctions between hepatocytes. Moreover, the spatial organization of ER-PM contacts is conserved in epithelial spheroids, suggesting that ER-PM contacts may serve conserved roles in epithelial cell architecture. Consistent with this notion, we show that ORP5 activity at ER-PM contacts modulates apical-basolateral aspect ratio in HepG2 cells. Thus, ER-PM contacts have a conserved distribution and crucial roles in PM domain architecture across epithelial cell types.

Introduction

The liver is composed mostly of polarized epithelial cells known as hepatocytes. Hepatocytes perform vital functions such as bile production and secretion, glucose and lipid metabolism, and detoxification of blood (Gissen and Arias, 2015; Schulze et al., 2019; Treyer and Musch, 2013). Hepatocytes have clearly defined apical, basal, and lateral PM domains that enable them to perform their diverse functions (Gissen and Arias, 2015; Musch, 2014; Schulze et al., 2019; Treyer and Musch, 2013). The apical domains of hepatocytes form bile canaliculi (BC) and are sites for polarized delivery of bile salt and lipid transporters. The basal (sinusoidal) domains of hepatocytes are exposed to blood for insulin signalling, nutrient uptake, and

protein secretion. The lateral domains flank the BC and form cell-cell junctions, including tight junctions that maintain the bile-blood barrier that specifies these distinct physiological processes. Defects in PM domain specification in hepatocytes are associated with various disorders such as bile secretory failure (cholestasis), fatty liver disease (steatosis), hepatocellular carcinoma progression, and hepatitis virus C entry (Gissen and Arias, 2015; Schulze et al., 2012; Wang and Boyer, 2004). Thus, it is important to understand how PM domain organization is established and maintained in hepatocytes.

ER-PM contacts have been proposed to serve critical roles in the control of PM lipid composition and calcium (Ca^{2+}) dynamics (Balla et al., 2020; Chang et al., 2017; Liu et al., 2019; Stefan, 2020). For instance, the oxysterol-binding protein related protein 5 (ORP5, also named OSBPL5) has been shown to localize to ER-PM contacts and regulate levels of phosphatidylserine, phosphatidylinositol 4-phosphate, and phosphatidylinositol 4,5-bisphosphate at the PM (Chung et al., 2015; Ghai et al., 2017; Sohn et al., 2016; Sohn et al., 2018). As these anionic phospholipids are proposed play important roles in PM domain organization, ORP5 and other protein activities at ER-PM contacts may fine-tune PM domain organization in hepatocytes and other epithelial cells. However, while the discovery and function of ER-mitochondrial contacts in hepatocytes are appreciated (Bernhard and Rouiller, 1956; Vance, 1990) the architecture and distribution of ER-PM contacts in hepatocytes have been overlooked. Moreover, while the anatomical detail of ER-PM contacts in muscle and neurons are well described (Fernandez-Busnadiego et al., 2015; Hayashi et al., 2008; Henkart et al., 1976; Porter and Palade, 1957; Rosenbluth, 1962; Sun et al., 2019; Wu et al., 2017), ultrastructural analyses of ER-PM contacts in epithelial tissues are lacking.

Here, we report the first quantitative electron microscopy (EM) analysis of ER-PM contacts in hepatocytes in mouse liver. We find distinct types of ER-PM contacts associated with specific PM domains. One class has a punctate morphology and are associated with the base of microvilli, whereas another class is extensive in size and are primarily observed at the lateral domain just outside the tight junctions. We observe the same patterns in epithelial spheroids using mouse renal inner medullary collecting duct (mIMCD) and Madin-Darby canine kidney (MDCK) cells, indicating that ER-PM contact organization and distribution are conserved along the apical-basolateral axis in polarized epithelial cells. Furthermore, we show that ORP5 activity at ER-PM contacts regulates apical-basolateral aspect ratio in HepG2 cells. Altogether, our findings suggest conserved roles of ER-PM contacts in specifying PM domain organization in epithelial cells.

Results

Quantitative ultrastructure analysis of ER-PM contacts in hepatocytes

To examine the quantity, size, and distribution of ER-PM contacts in an epithelial tissue, we conducted a comprehensive EM analysis of ER-PM contacts in hepatocytes from mouse liver (Figure 1). The hepatocyte PM is classified into three domains (Figure 1A). The apical domain forms the bile canaliculi (BC) that are bounded by the tight junctions; the basal domain refers to the PM exposed to the Space of Disse and sinusoids; the lateral domain forms inter-cellular junctions between two hepatocytes (H/H junctions). Figure 1A shows the average proportion (length %) of different PM domains in murine hepatocytes. The PM is partitioned into approximately equal portions of the basal (40%) and lateral (47%) domains, whereas only 13% of the PM is apical, resulting in an apical to basolateral (A/BL) aspect ratio of 0.15 (Figure 1A).

Next, we compared the extent of ER-PM contacts in each PM domain. The workflow for the quantitative analysis of ER-PM contacts is summarized in Supplemental Figure S1A. Approximately 20% of the PM is associated with the ER in the lateral domain that forms H/H junctions, nearly 4 times and 40 times more than that found in the basal (5.4%) and the apical (0.6%) domain respectively (Figure 1B, left panel). ER-mitochondrial and ER-lipid droplet contacts are also found in the sub-lateral cytoplasmic region (Figure 1A, Figure 2A, and Supplemental Figure S2A). The mean length of ER-PM contacts in the lateral domain that forms H/H junctions is 120 nm, which is significantly longer than that found in the basal (80 nm) and the apical (50 nm) domains (Figure 1B, middle panel). An example of a punctate ER-PM contact in the apical domain is shown in Figure 1C (and see Figure 2A and Supplemental Figure S2A for additional examples). While the apical domain displayed the lowest degree of ER-PM contact formation, the sub-apical cytoplasm is not devoid of the ER network *per se* and ER-associated vesicular compartments are observed in the sub-apical cytoplasmic region (Figure 1A). The reduced number and length of ER-PM contacts at the apical PM may be due to the presence of a thick actin cortex at the apical membrane (Figure 1A). Taken together, the initial results of the EM analyses suggest the morphology of ER-PM contacts is PM domain-specific and this may contribute to hepatocyte development and function.

To gain further insight into the arrangement and features of ER-PM contacts in hepatocytes, we measured the length of individual ER-PM contacts in each of the PM domains. A subpopulation of extensive ER-PM contacts (> 200 nm) was predominantly found in the lateral domain that forms H/H junctions (see the box and whisker plot in Figure 1B, right panel, and the histogram in Supplemental Figure S1B). Interestingly, most (~ 60%) of the extensive ER-PM contacts locate within 2 μm of the BC, and there is a steep drop in the

number of extensive ER-PM contacts as the distance from the tight junction increases (Figure 1D). These observations suggest that the formation and distribution of extensive ER-PM contacts is not a random event but under precise regulation.

3D reconstruction of ER-PM contacts in hepatocytes

Our 2D EM analysis indicated that distinct ER-PM contacts form in different PM domains. To confirm our initial observations, we examined the size and distribution of ER-PM contacts in 3D reconstructions of serial EM sections (Figure 2 and Supplemental Figure S2). This allowed a more detailed analysis of ER-PM contact morphological features such as area and shape. The PM (cyan), the ER (yellow), and ER-PM contacts (magenta) were manually traced in *xy* in each section, reconstructed into 3D models, and displayed as *xz* projections (Figure 2 and Supplemental Figure S2). 3D renderings of the ER-PM contacts and associated PM are provided in Supplemental Videos 1 and 2; corresponding versions additionally displaying segmented ER are provided in Supplemental Videos 3 and 4. Rare, punctate ER-PM contacts were observed at the base of microvilli in the apical domain (Figure 2A, asterisks*). Within the lateral domain, ER-PM contacts formed outside (adjacent to) the tight junctions that seal the BC and thus may primarily spatially associate with H/H junctions formed by adherens junctions, desmosomes, and gap junctions that reside within a few microns of the BC (Figure 2A and Supplemental Figure 2A). ER-PM contacts in the lateral domain were large and extensively occupied the PM (Figure 2A, chevrons >>). Some ER-PM contacts in this region even extended throughout the entire *z* series. Accordingly, the morphology of the cortical ER at the lateral domain resembled sub-surface cisternae (Figure 2A, Supplemental Figure S2A and Supplemental Video 3). The basal domain had a mixed population of ER-PM contacts, as both punctate and extensive contacts were observed (Figure 2B, # marks an example of an extensive contact). However, ER-PM contacts in the

basal domain were often smaller in size than those found in the lateral domain that forms H/H junctions (Figure 2A and 2B, bottom panels). In addition, punctate ER-PM contacts were often in the vicinity of protrusions and intrusions of the basal PM (Figure 2B, Supplemental Figure S2B and Video 4), similar to punctate ER-PM contacts at the base of microvilli in the apical domain.

Quantitative and statistical analyses revealed a prominent divergence in the size of ER-PM contacts between the different PM domains (Figure 3). The mean area of ER-PM contacts was significantly larger in the lateral domain that forms H/H junctions (10,674 nm^2) as compared to the basal (5748 nm^2) and apical (2534 nm^2) domains (Figure 3A). Accordingly, the maximal ER-PM contact area in the apical domain was an order of magnitude less than the max contact area in the basal and lateral (H/H) domains (see the table in Figure 3A). The extensive ER-PM contacts, especially those larger than 20,000 nm^2, were predominantly found in the lateral domain that forms H/H junctions (Figure 3B). Overall, our quantitative 2D and 3D EM analyses demonstrate that ER-PM contacts with different sizes and architectures are formed and distributed in specific PM domains. This raises the possibility that morphologically discrete ER-PM contacts may specify PM domain organization necessary for hepatocyte architecture and physiology.

To further characterize ER-PM contacts in hepatocytes, we examined additional features including the distance between the ER and the PM as well as the width of the cortical ER lumen at distinct PM domains (apical, lateral, basal). As assessed from the serial EM sections, a large proportion (45%) of ER-PM contacts at the lateral domain (H/H junctional domain) appeared to have an inter-membrane space of 10 to 15 nm, but spanned distances from 5 to 35 nm (Figure 3C). ER-PM contacts in the basal domain displayed a broad

distribution of inter-membrane spaces across sizes ranging from 5 to 30 nm (Figure 3C). These results are within previously reported values of inter-membrane space at ER-PM contacts (Fernandez-Busnadiego, 2016). Specific ER-PM inter-membrane distances have been ascribed to particular proteins, including the STIM1 and E-Syt1 proteins that form ER-PM contacts with an inter-membrane space of less than 20 nm (Fernandez-Busnadiego et al., 2015). The hepatic ER-PM contacts with an apparent spacing of 10-15 nm at the lateral domain (H/H junctional domain) may correspond to a specific protein such as STIM1. However, given the broad range of inter-membrane distances (5 to 35 nm), ER-PM contacts at the H/H junctional zone may be populated by a number of proteins that form and function at these sites. We also analyzed the width of the lumen of PM-associated ER and PM-free ER (Figures 3D and 3E). The lumen of PM-associated ER was significantly thinner that PM-free ER independent of PM domain (apical, basal, lateral). Previous studies have reported thinning of the cortical ER at ER-PM contacts in primary neurons as well as tissue culture cells overexpressing the STIM1 protein (Orci et al., 2009; Wu et al., 2017). While these data highlight trends between the ER-PM contacts in different PM domains, caution should be taken when interpreting absolute distances with nm accuracy and working with aldehyde fixed tissues.

ORP5 modulates BC morphology and apical-basolateral aspect ratio

To address roles of ER-PM contacts in hepatocytes, we took advantage of an in vitro cell culture system that resembles features of hepatocyte architecture in vivo. HepG2 cells polarize and form BC-like structures between the opposing apical membranes of cell couplets (Chiu et al., 1990). First, we categorized the development of HepG2 couplets into three consecutive stages based on BC morphology using a $PI(4,5)P_2$ (phosphatidylinositol 4,5-bisphosphate) reporter or the membrane dye CellMask as markers of the PM (see Figure 4A,

Supplemental Figure S3A and Figure 6A). The apposition stage refers to initial inter-cellular adhesion between two cells in a couplet. The developing BC stage appears as a globular accumulation of apical membrane at sites of PM apposition, as assessed by confocal microscopy. This is likely due to crowding of microvilli between the developing apical domains of the opposing cells. Accordingly, the relative CellMask signal was greater in developing BC than mature BC and sites of PM apposition (Supplemental Figure S3B). Furthermore, serial EM sections of a developing BC from a HepG2 couplet confirmed the presence of crowded microvilli between the developing apical domains (Supplemental Video 5 and Supplemental Figure S3C). A mature BC is defined by a dilated lumen and the presence of clearly resolved microvilli along the edges of hemi-canaliculi.

To address whether ER-PM contact proteins regulate PM domain organization in HepG2 cells, we initially focused on the well-characterized ORP5 protein which has been shown to localize to ER-PM contacts where it transports PS (phosphatidylserine) to the PM in exchange for PI4P (phosphatidylinositol 4-phosphate) and has been implicated in the regulation of PS, PI4P, and PI(4,5)P_2 at the PM (see Supplemental Figure S4A) (Chung et al., 2015; Ghai et al., 2017; Sohn et al., 2016; Sohn et al., 2018). ORP5 and its related protein ORP8 are expressed in liver and HepG2 cells (Jaworski et al., 2001; Li et al., 2016; Yan et al., 2008). Yet, roles of ORP5 exchange activity at ER-PM contacts in hepatocytes have not been addressed. We overexpressed mCherry-tagged wild type ORP5 or a mutant form lacking its PH domain, ORP5ΔPH, that does not localize to ER-PM contacts (Ghai et al., 2017) (Supplemental Figures S4A and S4B) and assessed their impact on HepG2 couplet development (Figures 4B and 4C). Expression of wild type ORP5 impaired BC development as shown by the PI(4,5)P_2 probe GFP-PLCδ-PH that served as a PM marker (Figure 4B). The fraction of cell couplets in the apposition stage increased (1.3-fold) while the fraction of the

developing and mature BC stages decreased (2-fold and approximately 5-fold, respectively; Figure 4C) In contrast, expression of the mutant ORP5ΔPH protein, that does not localize to ER-PM contacts, had no major effects on BC development (Figures 4B and 4C). Likewise, expression of a mutant form of ORP5 that localizes to ER-PM contacts but is impaired in PS/PI4P exchange due to substitutions in its ORD domain (H478A, H479A) (Chung et al., 2015; Du et al., 2020) (Supplemental Figure S4A) did not delay BC development (Figures 4E and 4F). As an additional control, we examined the effect of expression of E-Syt1 that has been shown to populate and induce ER-PM contacts as well as transfer lipids at these sites (Fernandez-Busnadiego et al., 2015; Saheki et al., 2016). Unlike ORP5, expression of mCherry-tagged E-Syt1 did not affect BC development (Supplemental Figures S4C and S4D). We also measured the aspect ratio between apical and basolateral domains as an additional parameter. Hepatocytes in mouse liver and mature HepG2 couplets have a similar apical to basolateral aspect ratio (A/BL ratio = 0.15; see Figures 1A, 4D, and 6B). The A/BL aspect ratio was reduced in HepG2 couplets expressing the wild type ORP5 protein, but not the mutant ORP5ΔPH protein (Figure 4D). Thus, ORP5 lipid exchange activity at ER-PM contacts modulates BC morphology and A/BL aspect ratio.

We employed correlative light and electron microscopy (CLEM) to determine the effect of ORP5 expression on ER-PM contacts. We compared ER-PM contacts at sites of cell-cell apposition in HepG2 couplets where one cell in the couplet expressed either GFP, GFP-ORP5, or GFP- ORP5ΔPH (Figure 5, A–C). GFP-ORP5 expression consistently increased the extent of ER-PM association (Figure 5B, orange arrows), as much as 8-fold greater than the opposing cell not expressing GFP-ORP5 (Figure 5D). In contrast, GFP alone and GFP-ORP5ΔPH had no distinguishable impact on ER-PM association (Figures 5A, 5C, and 5D). Accordingly, ER-PM association was 4-fold greater at sites of cell-cell apposition in cells

expressing GFP-ORP5 as compared to cells expressing GFP alone or GFP-ORP5ΔPH (Supplemental Figure S4E).

To better understand ORP5 function in PM domain organization, we depleted ORP5 and its related protein ORP8 using siRNA. Knockdown of ORP5 and ORP8 expression was confirmed by RT-qPCR (Supplemental Figure S5). Double knockdown of ORP5 and ORP8 led to a statistically significant increase in the apical to basolateral (A/BL) aspect ratio as well as a slight increase in BC diameter (Figures 6B and 6C). BC development was not delayed upon depletion of ORP5 and ORP8 (Supplemental Figure S5C). If anything, there was even a slight increase in the proportion of couplets with developing BC and a corresponding decrease in couplets at the cell-cell apposition stage (Supplemental Figure S5C). Thus, ORP5 and ORP8 are not required for apical domain formation and BC development. Instead, ORP5 (and possibly ORP8) appears to modulate the proportion of apical and basolateral membrane domains.

Certain phosphoinositide isoforms are proposed to serve as spatial cues for apical-basolateral domain identity in epithelial cells (Martin-Belmonte et al., 2007; Roman-Fernandez et al., 2018; Shewan et al., 2011). In particular, $PI(4,5)P_2$ is proposed to be enriched in the apical domain of polarized MDCK cells (Martin-Belmonte et al., 2007; Roman-Fernandez et al., 2018) where it may serve as a determinant in apical domain identity and function (Shewan et al., 2011). However, it is not known whether $PI(4,5)P_2$ is enriched in the apical domain of hepatocytes. Moreover, it is not known whether or how ER-PM contacts regulate $PI(4,5)P_2$ in order to modulate PM domain organization, including A/BL aspect ratio, in hepatocytes or other epithelial cells. We performed ratiometric imaging using the $PI(4,5)P_2$ reporter GFP-PLCδ-PH and CellMask as a general PM dye (Figure 6D). This approach revealed that the

$PI(4,5)P_2$ reporter was enriched at the apical domain as compared to basolateral domains in HepG2 cells with mature BC (3-fold; Figure 6D). Depletion of both ORP5 and ORP8 led to a significant decrease in the apical to basolateral $PI(4,5)P_2$ reporter gradient (1.5-fold lower, as compared to control cells; Figure 6D). Because ORP5 is implicated in the regulation of PI4P and PS at the PM as well as $PI(4,5)P_2$ (see Supplemental Figure S6A) (Chung et al., 2015; Ghai et al., 2017; Sohn et al., 2016; Sohn et al., 2018), we measured the specific intensity of PI4P, $PI(4,5)P_2$, and PS reporters at different PM domains upon double knockdown of ORP5 and ORP8 (Supplemental Figure S6). The signal of the $PI(4,5)P_2$ reporter increased in all PM domains upon depletion of both ORP5 and ORP8 whereas the PS reporter signal decreased (Supplemental Figure S6). Curiously, the PI4P reporter signal increased only slightly (but not significantly) at the lateral domain but not the apical and basal domains upon ORP5 and ORP8 depletion (Supplemental Figure S6B). Previous studies have indicated that PI4P is rapidly converted to $PI(4,5)P_2$ at the PM (Myeong et al., 2021; Willars et al., 1998), and this may explain the measurable increase in the $PI(4,5)P_2$ reporter but not the PI4P reporter. Altogether, the results suggest that ORP5 and ORP8 may modulate the apical to basolateral aspect ratio in HepG2 cells (Figures 4D and 6B) at least in part by regulating $PI(4,5)P_2$ (Figure 6D and Supplemental Figure S6C).

The organization of ER-PM contacts is conserved in epithelial spheroids

To determine whether the morphology and distribution of ER-PM contacts are conserved in epithelial cells, we also examined 3D epithelial cell culture systems. We performed quantitative EM analyses, identical to that done on hepatocytes, on spheroids developed from mouse renal inner medullary collecting duct (mIMCD) cells and Madin-Darby canine kidney cells (MDCK) (Figures 7 and 8). The PM of individual cells in the spheroids were classified into three domains: the apical PM facing the enclosed lumen, the basal PM facing the

external gel matrix, and the lateral PM domain that forms cell-cell junctions (Figures 7A and 8A).

The proportion of each PM domain in the IMCD spheroids was similar to hepatocytes, with equal portions of basal (38%) and lateral (39%) domains and the apical domain in least abundance (23%). The organization of ER-PM contacts in mIMCD spheroids also resembled those observed in hepatocytes from mouse liver. The lateral domain that forms cell-cell junctions was significantly ER-associated (8.3% of PM associated with ER, Figure 7B left panel; see Supplemental Figure S7A for more examples of abundant ER-PM contacts at the lateral PM domain). This coverage (% of PM associated with ER) was 4 times more abundant than that observed in the apical domain (1.7%) and 8-fold greater than the basal domain (1.0%) (Figure 7B, left panel). Similar to hepatocytes, ER-PM contacts were significantly longer in the lateral domain than those in the apical and the basal domains (Figure 7, middle panel). Moreover, extensive ER-PM contacts (>200 nm) were primarily observed at the lateral domain (as shown by the box and whisker plot, Figure 7B right panel, and the histogram in Supplemental Figure S7B), similar to hepatocytes. Furthermore, the majority of the extensive ER-PM contacts located within 5 μm of the tight junction (Figure 7D), similar to hepatocytes.

Cells in MDCK spheroids formed smaller lateral domains (23%) and relatively larger basal (47%) and apical (30%) domains than IMCD spheroids, possibly because the MDCK spheroids examined have a larger lumen (Figure 8A). Yet the organization and distribution of ER-PM contacts in MDCK spheroids resembled those observed in IMCD spheroids and hepatocytes from mouse liver. The lateral domain that forms cell-cell junctions displayed the highest ER association (7.1% of the PM associated with the ER, Figure 8B left panel), 35-

fold greater than that observed in the apical domain (0.2%) and more than 3-fold in the basal domain (2.0 %) (Figure 8B left panel). Accordingly, ER-PM contacts were more abundant in the lateral domain (n = 65) than the apical domain (n = 4) (Figure 8B right panel and Supplemental Figure S5C), similar to hepatocytes and IMCD spheroids. Even while the mean length of ER-PM contacts was similar among the different PM domains in MDCK spheroids (Figure 8B), extensive ER-PM contacts (>200 nm) were not found at the apical domain and only observed in the lateral and basal domains (Figure 8B and Supplemental Figure S7C). Finally, the extensive ER-PM contacts were located within 6 μm of the tight junction (Figure 8C), similar to hepatocytes and mIMCD spheroids. Thus, the morphological features and distribution of ER-PM contacts, particularly the presence of extensive ER-PM contacts in the lateral domain that forms cell-cell junctions, are conserved in epithelial cells.

Discussion

The organization of ER-PM contacts is conserved in polarized epithelial cells

Despite the discovery of ER-PM contacts decades ago (Henkart et al., 1976; Porter and Palade, 1957; Rosenbluth, 1962) there has been no thorough morphological characterizsation of ER-PM contacts in an epithelial tissue. Moreover, while the anatomical detail of junctional complexes in epithelial cells (Farquhar and Palade, 1963) and bile canaliculi (BC) in hepatocytes (Jeejeebhoy et al., 1980; Oda et al., 1974; Phillips et al., 1974; Phillips et al., 1976) have been described, striking features of ER-PM contacts in polarized epithelial cells have been overlooked. Our EM analyses provide the first detailed quantitative information on ER-PM contacts in distinct PM domains (apical, lateral, and basal) of hepatocytes from mouse liver and epithelial spheroids. The quantity, size, and architecture of ER-PM contacts differ between each of the PM domains. ER-PM contacts are scarce and punctate at the apical

PM, possibly due to a thick actin cortex in this region (Figure 1A). Accordingly, previous studies have reported coordination between ER-PM contacts and the actin cytoskeleton (Hartzell et al., 2016; Hsieh et al., 2017; van Vliet et al., 2017). In contrast, ER-PM contacts are more abundant and extensive at the lateral domains where cell-cell junctions form (Figures 1–3, 7 and 8; Supplemental Figures S2 and S7). This pattern in ER-PM contact distribution is conserved in hepatocytes and epithelial spheroids and may even be conserved throughout evolution. ER-PM contact anisotropy has been described in budding and fission yeast where sites of polarized growth have fewer ER-PM contacts compared to mother cells or the lateral PM domains respectively, particularly in the G1 phase of the cell cycle when polarized growth is most prominent (Ng et al., 2018; West et al., 2011).

ER-PM contacts in the apical and basolateral domains of epithelial cells display distinct architectures. Punctate ER-PM contacts at the apical domain are formed by cortical ER tubules and extensive ER-PM contacts are formed in the lateral domain by flat subsurface ER cisternae (Figures 1 and 2A; Supplemental Figure S2A; Supplemental Video 3). Punctate ER-PM contacts are often found at the base of microvilli in the apical domain or at the base of curved membranes in the basal domains, suggesting a relationship with local PM curvature and the extent of ER-PM association. Punctate ER-PM contacts have also been observed at the base of microvilli in *Drosophila* photoreceptor cells (Suzuki and Hirosawa, 1994). In contrast, extensive ER-PM contacts are associated with planar regions of the lateral PM domain. The majority of the extensive ER-PM contacts in epithelial cells localize within a few microns of the tight junctions (Figures 1D, 7C, and 8C), implying they may function in defining the apical boundary and tight junction positioning or they may regulate junctional complexes in the lateral domains (see below for further discussion).

ORP5 activity at ER-PM contacts defines apical to basolateral aspect ratio

Our findings indicate that ORP5 modulates apical to basolateral aspect ratio (Figures 4 and 6). ORP5 is reported to carry out PI4P/PS exchange at ER-PM contacts, and ORP5 inhibition is reported to increase PI4P and PI(4,5)P_2 at the PM whereas overexpression of ORP5 lowers PI4P and PI(4,5)P_2 at the PM (Chung et al., 2015; Ghai et al., 2017; Sohn et al., 2016; Sohn et al., 2018). Likewise, we found that depletion of both ORP5 and ORP8 resulted in increased localization of a PI(4,5)P_2 reporter at the PM (Supplemental Figure S6). Many apical proteins contain polybasic motifs that prefer highly negative charged membrane surfaces containing PI4P, PI(4,5)P_2, and PS (Krahn, 2020; Shewan et al., 2011). PI(4,5)P_2 has a greater negative charge valence (-4) than PS (-1) (Slochower et al., 2014). Through the removal of PI4P in exchange for PS at ER-PM contacts, ORP5 may limit PI4P and PI(4,5)P_2 levels in the lateral domain and contribute to the differential surface charge density between the apical and lateral domains. Accordingly, depletion of ORP5 and ORP8 disrupted the apical to basolateral PI(4,5)P_2 gradient in HepG2 couplets with mature BC (Figure 6D). In addition, ORP5 activity may define PM domain organization by regulation of PS distribution or metabolism. Future experiments are needed to test whether ORP5 specifies the apical domain boundary or lateral domain stability by regulating membrane lipid composition and net charge.

Our results indicate that ORP5 function at ER-PM contacts modulates BC development and size. ORP5 is also proposed to function at ER-mitochondrial contacts (Galmes et al., 2016) that are implicated in phospholipid metabolism in hepatocytes (Vance, 1990). Similarly, ORP5 has been implicated at ER-lipid droplet contacts (Du et al., 2020), and ORP5 overexpression may alter ER-lipid droplet dynamics. However, expression of a mutant ORP5 protein lacking its PH domain had no effect on BC development or apical aspect ratio (Figure 4). The ORP5 PH domain is necessary for ORP5 localization and function at ER-PM contacts

(Chung et al., 2015; Sohn et al., 2018), but is not implicated in ORP5 targeting to ER-mitochondrial or ER-lipid droplet contacts (Du et al., 2020; Galmes et al., 2016). Furthermore, expression of a mutant form of ORP5 that localizes to ER-PM contacts but is impaired in PS/PI4P exchange due to substitutions in its ORD domain (H478A, H479A) (Chung et al., 2015; Du et al., 2020) did not affect BC morphology (Figures 4E and 4F). Taken together, these results indicate that ORP5 activity at ER-PM contacts modulates apical to basolateral aspect ratio.

Extensive ER-PM contacts are associated with lateral domains

As mentioned, the majority of extensive ER-PM contacts are at the lateral domain within a few microns of the apical boundary in both hepatocytes and epithelial spheroids (Figures 1, 7, and 8). As ER-PM contacts are enriched at lateral domains that form cell-cell junctions, it is reasonable to postulate that they may participate in inter-cellular communication or the regulation of junctional complexes in the lateral domains. Consistent with this notion, ORP5 activity at ER-PM contacts appeared to promote or stabilize cell-cell junctions (PM apposition stage between HepG2 couplets, Figure 4). As such, regulation of membrane lipid and Ca^{2+} dynamics at extensive ER-PM contacts may control junctional complexes in the lateral domain. The dynamics and function of tight junctions, adherens junctions, gap junctions, and desmosomes are proposed to be modulated by membrane lipid composition, particularly cholesterol and $PI(4,5)P_2$ content (Chen-Quay et al., 2009; Nusrat et al., 2000; Shigetomi et al., 2018; van Zeijl et al., 2007; Zimmer and Kowalczyk, 2020). ORP family members perform diverse biological functions including cholesterol transport (Olkkonen, 2015; Raychaudhuri and Prinz, 2010). It will be interesting to address roles of ORP family members and additional lipid transfer proteins in the formation and remodelling of junctional complexes (tight junctions, adherens junctions, gap junctions, and desmosomes) as well as

the planar PM morphology that is observed at extensive ER-PM contacts within the lateral domain.

In conclusion, morphologically distinct ER-PM contacts are conserved in epithelial cells: rare punctate contacts at the apical domain and extensive contacts in the lateral domain. Beyond PM domain architecture, it will be exciting to examine roles of ER-PM contacts in vital hepatocyte functions including bile production and secretion, lipid regulation, steroid metabolism, insulin signalling, and glucose homeostasis. As our findings suggest that the arrangement of ER-PM contacts is conserved in epithelial cells, it will be interesting to further examine the physiological roles of ER-PM contacts in additional epithelial tissues. In this regard, it is intriguing to consider whether remodelling of ER-PM contacts is involved in epithelial cell and tissue morphogenesis during normal development or disease such as the epithelial to mesenchymal transition during cancer progression.

Materials and Methods

Reagents

Cells lines, plasmids, antibodies, and primers used in this study are listed in Supplemental Table 1, 2, 3, and 4 respectively.

Cell culture and maintenance

HepG2 cells were cultured and maintained in Dulbecco's Modified Eagle Medium/Nutrient Mixture F-12 (DMEM/F12; Life Technologies). Media were supplemented with 10% (v/v) fetal bovine serum (FBS, Life Technologies), 100 U/mL of penicillin and 100 μg/mL of

streptomycin at 37°C and 5% CO_2. The cells were grown in a humidified incubator and passaged in a 1:15 ratio every 3 days or upon 90% confluency.

mIMCD cells were cultured following the protocol described in (Banushi et al., 2016). For IMCD spheroid formation, the cells were cultured on an 8-well chamber slide (Lab-Tek) in DMEM/F12 supplemented with 2% FBS. The cells were sandwiched with Geltrex according to the manufacturer's protocol (Life Technologies), and 2 x 10^4 cells were seeded per well and grown at 37°C for 4 days to form spheroids.

MDCK spheroids were developed on an 8-well chamber slide (Lab-Tek) following an "on-top" culture protocol modified from Jaffe et al. (2008). The 8-well chamber was pre-coated with 2% Matrigel (Corning), and once solidified suppled with trypsin-treated cells in complete DMEM media mixed with 2% Matrigel. 10,000 cells were seeded per well and grown at 37°C for 6 days to form spheroids.

Acquisition of mouse liver samples

Mouse liver samples used for EM analysis were obtained from a previous study (Hanley et al., 2017). Briefly, male mice were sacrificed at age 14 weeks and livers were harvested as described (Hanley et al., 2017). For the Hanley et al. 2017 study, all animals were housed in accordance with the UK Home Office guidelines and the tissue harvesting was carried out in accordance with the UK Animal (Scientific Procedures) Act 1986. No additional animals were used during the course of the current study.

Transmission electron microscopy (TEM) of hepatocytes from mouse liver and 3D spheroids

A piece of liver (approximately 8mm x 8mm x 3mm) was injection fixed with warm 1.5% glutaraldehyde in 1% sucrose 0.1M sodium cacodylate and left up to 20 minutes. Once firm and fixed, the tissue was cut into 100 µm thick slices using a vibrating microtome. 2D hepatocyte and 3D IMCD or MDCK cultures were fixed with 2% EM grade formaldehyde (TAAB) and 1.5% EM grade glutaraldehyde (TAAB) in either PBS or 0.1M sodium cacodylate. All samples were incubated for 1 hour in 1% osmium tetroxide/1.5% potassium ferricyanide at 4°C before being treated with 1% tannic acid in 0.05M sodium cacodylate (45 mins). Samples were then dehydrated through an ethanol series and embedded in Epon resin (TAAB). Ultrathin sections, 70nm, were collected on formvar coated slot grids using an Ultramicrotome (Leica), stained with lead citrate before being imaged using an 120kV Transmission electron microscope (Thermo Fisher Scientific) and images were captured using iTEM software and a Morada CCD camera (OSIS).

Correlative light and electron microscopy (CLEM) of HepG2 couplets

Live cell imaging was performed as described below using either the Ultraview Vox spinning disc microscope. Once a desired developmental stage had been identified, the cells were fixed in 4% EM grade formaldehyde (TAAB) in 0.1M sodium cacodylate to locate the grid number and position of the cells. Secondary fixation was performed in 1.5% glutaraldehyde/2% formaldehyde in 0.1M caco for 30–60 min. The sample preparation then followed a modified NCMIR SBFSEM protocol (Deerinck et al., 2010) Briefly, the cells were post-fixed in 1.5% potassium ferricyanide/1% osmium tetroxide for one hour, and then incubated in 1% filtered

thiocarbohydrazide for 20 min. The cells followed another 2% osmium tetroxide and 1% UA treatment with several washes between each step. The cells then were counterstained with lead aspartate and dehydrated through an ascending series of ethanol to 100% prior to infiltration with Epoxy resin and polymerisation overnight at 60°C. Sections were collected and imaged as above.

Image analysis

Quantification of ER-PM contacts in tissues and organoids:

EM images were formatted and analyzed using Fiji (Schindelin et al., 2012) (RRID: SCR_002285) and its inbuilt Straighten plugin (Kocsis et al., 1991). See Figure S1A for the analysis workflow that quantified the PM category and physical parameters of the ER-PM contacts in hepatocytes and IMCD or MDCK spheroids. For Figures 1 and 3, distances of 20 nm or less between the PM and ER were scored as contacts; For Figure 1, distances of 20 nm or less between the PM and ER were scored as contacts; for Figure 3C, distances of 40 nm or less between the PM and ER were scored as contacts;

Segmentation of ultrastructure:

Serial micrographs were stacked and aligned using the ImageJ StackReg Registration plugin (Thevenaz et al., 1998) and manual segmentation was done using Amira (Thermofisher Scientific; RRID:SCR_007353). The voxels of PM, ER, and ER-PM contacts were manually traced based on their electron density, morphological features, and the continuum of associated physical parameters. Segmented structures were rendered into 3D models using Amira and exported into videos with a speed of 25 frames per second.

Confocal microscopy

Fluorescent microscopy was performed on a TCS SP5 microscope with Leica Application Suite: Advanced Fluorescence (LAS AF; RRID:SCR_013673) software. For live imaging, cells were kept at 37°C with 5% CO2 in the Pe-Con stage-top incubation system throughout the imaging process and a 63x oil-immersion objective (NA = 1.4) was used for image acquisition. Alternatively, the image was acquired using an Ultraview Vox spinning disc microscope operating on a Volocity interface (RRID:SCR_002668) with a C9100-13 EMCCD camera as the detector. A 60x oil-immersion objective (NA = 1.4) was used.

DNA Transfection

HepG2 cells were seeded at a density of 65,000 - 75,000 cells per 35mm dish (day 0) and grown overnight before a 24h transfection. Plasmids were introduced using Lipofectamine 3000 (Life Technologies) according to the manufacturer's instructions. 0.5 μg of DNA plasmids expressing various lipid biosensors and/or proteins of interest was used per dish. Thereafter, confocal imaging or cell lysis was subsequently done (day 2).

RNA Transfection

Lonza Cell Line Nucleofector kit V was used to introduce endoribonuclease-prepared siRNA targeting ORP5 (Cat no. EHU085181-20UG) and ORP8 (Cat no. EHU070271-20UG) in HepG2 cells. Alternatively, Lipofectamine RNAiMAX (Life Technologies) was used to introduce siRNAs to the cells following manufacturer’s protocol. The esiRNA targeting *Renilla* Luciferase (Cat no. EHURLUC-20UG) was used as the control. Each reaction contains $1x10^6$ cells and 30nM siRNA. The H-022 program for high viability was selected. After the program, HepG2 cells were seeded at a density of 200,000 cells per 35mm dish for

72h before imagining.

Quantitative PCR analyses

RNAi transfected HepG2 cells were lysed in RLT buffer (Qiagen) and the extractions was performed using Qiagen RNeasy Plus kit (Cat: 74134) according to manufacturer guidelines. Purified RNA was stored at –80 °C before cDNA synthesis. First-strand cDNA synthesis was performed using Superscript reverse transcriptase IV (Invitrogen; Cat:18091050) following manufacturer's protocol. Quantitative PCR was carried out with validated or PrimerQuest designed primers (10 µM) in 25 µl reactions using the Platinum SYBR Green one-step qPCR kit (Invitrogen) and the following program: 50 °C for 2 min, 95 °C for 2 min, and 40 cycles of amplification at 95 °C for 15s and 60 °C for 45s. Relative amounts of target mRNA were compared with TATA-binding protein (TBP) and alpha-tubulin (TUBa) using the 2-ΔΔ Ct method, where the control cell-type or treatment group was normalized to 1. The primers used for the RT-qPCR tests are listed in Supplemental Table 4.

SDS-PAGE and immunoblotting

Cells were harvested using a cell scraper and were lysed with 200 µl/well of 0.1% CHAPS lysis buffer (50 mM Tris-HCl, 150 mM NaCl and 1 mM EDTA) supplemented with a Mini Protease inhibitor cocktail (Roche). The cell lysate was incubated on ice for 15 mins with occasional mixing before centrifugation at 20,000 g at 4°C for 10 min. The supernatant was collected and denatured in an SDS sample buffer at 99°C for 10 min before resolving on an 8% or 10% SDS-PAGE gel. Resolved proteins were then transferred to a supported nitrocellulose transfer membrane (GVS Filter Technology) in 10% methanol transfer buffer

(Geneflow). The membrane was blocked against nonspecific antibody binding using 5% milk in Tris-buffered saline (TBS) containing 0.05% Tween 20 (TBST) for at least 1 hour and then probed with primary antibodies at 4°C overnight and horseradish peroxidase (HRP)-conjugated secondary antibodies at room temperature for 1 hour. Chemiluminescence was visualised using the ImageQuant LAS 4000 system and exported as digitalised images.

Acknowledgements

We thank Pietro De Camilli, Tamas Balla, Jen Liou, and Rob Yang for reagents. We are grateful to Nathaniel Soh, Natalie Chui, Christa Benjamin, Chiara Mencarelli, Joanna Hanley, Rebecca Fiadeiro, and Ania Straatman-Iwanowska for expert technical assistance. We also thank Emily Eden, Tim Levine, Graham Warren, Dan Cutler, Mark Marsh, and Ffion Thomas for helpful discussions. P.G. was funded by the European Research Council, grant code ERC-2013-StG-337057. F.P. was funded by the MRC (MC_UU_12018/3), BBSRC (BB/R000697) and Royal Society (Award #181274). J.J.B. was supported by MRC funding to the MRC Laboratory of Molecular Cell Biology at UCL, award code MC_U12266B. C.J.S. was supported by MRC funding to the MRC Laboratory of Molecular Cell Biology University Unit at UCL, award code MC_UU_00012/6.

Author Contributions

G.H.C.C., M.L., P.G., F.P., J.J.B. and C.J.S. designed experiments; G.H.C.C. and J.J.B. performed experiments; G.H.C.C., J.J.B., and C.J.S. analyzed the data and wrote the manuscript. All authors discussed the results and commented on the manuscript.

Declaration of Interests

The authors declare no competing financial interests.

References

Balla, T., G. Gulyas, Y.J. Kim, and J. Pemberton. 2020. Phosphoinositides and Calcium Signaling. A Marriage Arranged in Er-Pm Contact Sites. *Curr Opin Physiol*. 17:149-157.

Banushi, B., F. Forneris, A. Straatman-Iwanowska, A. Strange, A.M. Lyne, C. Rogerson, J.J. Burden, W.E. Heywood, J. Hanley, I. Doykov, K.R. Straatman, H. Smith, D. Bem, J. Kriston-Vizi, G. Ariceta, M. Risteli, C. Wang, R.E. Ardill, M. Zaniew, J. Latka-Grot, S.N. Waddington, S.J. Howe, F. Ferraro, A. Gjinovci, S. Lawrence, M. Marsh, M. Girolami, L. Bozec, K. Mills, and P. Gissen. 2016. Regulation of post-Golgi LH3 trafficking is essential for collagen homeostasis. *Nat Commun*. 7:12111.

Bernhard, W., and C. Rouiller. 1956. Close topographical relationship between mitochondria and ergastoplasm of liver cells in a definite phase of cellular activity. *J Biophys Biochem Cytol*. 2:73-78.

Chang, C.L., Y.J. Chen, and J. Liou. 2017. ER-plasma membrane junctions: Why and how do we study them? *Biochim Biophys Acta Mol Cell Res*. 1864:1494-1506.

Chen-Quay, S.C., K.T. Eiting, A.W. Li, N. Lamharzi, and S.C. Quay. 2009. Identification of tight junction modulating lipids. *J Pharm Sci*. 98:606-619.

Chiu, J.H., C.P. Hu, W.Y. Lui, S.C. Lo, and C.M. Chang. 1990. The formation of bile canaliculi in human hepatoma cell lines. *Hepatology*. 11:834-842.

Chung, J., F. Torta, K. Masai, L. Lucast, H. Czapla, L.B. Tanner, P. Narayanaswamy, M.R. Wenk, F. Nakatsu, and P. De Camilli. 2015. INTRACELLULAR TRANSPORT. PI4P/phosphatidylserine countertransport at ORP5- and ORP8-mediated ER-plasma membrane contacts. *Science*. 349:428-432.

Deerinck, T.J., E.A. Bushong, A. Thor, and M.H. Ellisman. 2010. NCMIR methods for 3D EM: A new protocol for preparation of biological specimens for serial block face scanning electron microscopy. 6-8 pp.

Du, X., L. Zhou, Y.C. Aw, H.Y. Mak, Y. Xu, J. Rae, W. Wang, A. Zadoorian, S.E. Hancock, B. Osborne, X. Chen, J.W. Wu, N. Turner, R.G. Parton, P. Li, and H. Yang. 2020. ORP5 localizes to ER-lipid droplet contacts and regulates the level of PI(4)P on lipid droplets. *J Cell Biol*. 219.

Farquhar, M.G., and G.E. Palade. 1963. Junctional complexes in various epithelia. *J Cell Biol*. 17:375-412.

Fernandez-Busnadiego, R. 2016. Supramolecular architecture of endoplasmic reticulum-plasma membrane contact sites. *Biochem Soc Trans*. 44:534-540.

Fernandez-Busnadiego, R., Y. Saheki, and P. De Camilli. 2015. Three-dimensional architecture of extended synaptotagmin-mediated endoplasmic reticulum-plasma membrane contact sites. *Proc Natl Acad Sci U S A*. 112:E2004-2013.

Galmes, R., A. Houcine, A.R. van Vliet, P. Agostinis, C.L. Jackson, and F. Giordano. 2016. ORP5/ORP8 localize to endoplasmic reticulum-mitochondria contacts and are involved in mitochondrial function. *EMBO Rep*. 17:800-810.

Ghai, R., X. Du, H. Wang, J. Dong, C. Ferguson, A.J. Brown, R.G. Parton, J.W. Wu, and H. Yang. 2017. ORP5 and ORP8 bind phosphatidylinositol-4, 5-biphosphate (PtdIns(4,5)P 2) and regulate its level at the plasma membrane. *Nat Commun*. 8:757.

Gissen, P., and I.M. Arias. 2015. Structural and functional hepatocyte polarity and liver disease. *J Hepatol*. 63:1023-1037.

Hanley, J., D.K. Dhar, F. Mazzacuva, R. Fiadeiro, J.J. Burden, A.M. Lyne, H. Smith, A. Straatman-Iwanowska, B. Banushi, A. Virasami, K. Mills, F.P. Lemaigre, A.S. Knisely, S. Howe, N. Sebire, S.N. Waddington, C.C. Paulusma, P. Clayton, and P.

Gissen. 2017. Vps33b is crucial for structural and functional hepatocyte polarity. *J Hepatol*. 66:1001-1011.
Hartzell, C.A., K.I. Jankowska, J.K. Burkhardt, and R.S. Lewis. 2016. Calcium influx through CRAC channels controls actin organization and dynamics at the immune synapse. *Elife*. 5.
Hayashi, M., A. Raimondi, E. O'Toole, S. Paradise, C. Collesi, O. Cremona, S.M. Ferguson, and P. De Camilli. 2008. Cell- and stimulus-dependent heterogeneity of synaptic vesicle endocytic recycling mechanisms revealed by studies of dynamin 1-null neurons. *Proc Natl Acad Sci U S A*. 105:2175-2180.
Henkart, M., D.M. Landis, and T.S. Reese. 1976. Similarity of junctions between plasma membranes and endoplasmic reticulum in muscle and neurons. *J Cell Biol*. 70:338-347.
Hsieh, T.S., Y.J. Chen, C.L. Chang, W.R. Lee, and J. Liou. 2017. Cortical actin contributes to spatial organization of ER-PM junctions. *Mol Biol Cell*. 28:3171-3180.
Jaffe, A.B., N. Kaji, J. Durgan, and A. Hall. 2008. Cdc42 controls spindle orientation to position the apical surface during epithelial morphogenesis. *J Cell Biol*. 183:625-633.
Jaworski, C.J., E. Moreira, A. Li, R. Lee, and I.R. Rodriguez. 2001. A family of 12 human genes containing oxysterol-binding domains. *Genomics*. 78:185-196.
Jeejeebhoy, K.N., M.J. Phillips, J. Ho, and A. Bruce-Robertson. 1980. Ultrastructural and functional studies of cultured adult rat hepatocytes. *Ann N Y Acad Sci*. 349:18-27.
Kocsis, E., B.L. Trus, C.J. Steer, M.E. Bisher, and A.C. Steven. 1991. Image averaging of flexible fibrous macromolecules: the clathrin triskelion has an elastic proximal segment. *J Struct Biol*. 107:6-14.
Krahn, M.P. 2020. Phospholipids of the Plasma Membrane - Regulators or Consequence of Cell Polarity? *Front Cell Dev Biol*. 8:277.
Li, J., X. Zheng, N. Lou, W. Zhong, and D. Yan. 2016. Oxysterol binding protein-related protein 8 mediates the cytotoxicity of 25-hydroxycholesterol. *J Lipid Res*. 57:1845-1853.
Liu, H., A. Kabrah, M. Ahuja, and S. Muallem. 2019. CRAC channels in secretory epithelial cell function and disease. *Cell Calcium*. 78:48-55.
Martin-Belmonte, F., A. Gassama, A. Datta, W. Yu, U. Rescher, V. Gerke, and K. Mostov. 2007. PTEN-mediated apical segregation of phosphoinositides controls epithelial morphogenesis through Cdc42. *Cell*. 128:383-397.
Musch, A. 2014. The unique polarity phenotype of hepatocytes. *Exp Cell Res*. 328:276-283.
Myeong, J., C.G. Park, B.C. Suh, and B. Hille. 2021. Compartmentalization of phosphatidylinositol 4,5-bisphosphate metabolism into plasma membrane liquid-ordered/raft domains. *Proc Natl Acad Sci U S A*. 118.
Ng, A.Y.E., A.Q.E. Ng, and D. Zhang. 2018. ER-PM Contacts Restrict Exocytic Sites for Polarized Morphogenesis. *Curr Biol*. 28:146-153 e145.
Nusrat, A., C.A. Parkos, P. Verkade, C.S. Foley, T.W. Liang, W. Innis-Whitehouse, K.K. Eastburn, and J.L. Madara. 2000. Tight junctions are membrane microdomains. *J Cell Sci*. 113 (Pt 10):1771-1781.
Oda, M., V.M. Price, M.M. Fisher, and M.J. Phillips. 1974. Ultrastructure of bile canaliculi, with special reference to the surface coat and the pericanalicular web. *Lab Invest*. 31:314-323.
Olkkonen, V.M. 2015. OSBP-Related Protein Family in Lipid Transport Over Membrane Contact Sites. *Lipid Insights*. 8:1-9.

Orci, L., M. Ravazzola, M. Le Coadic, W.W. Shen, N. Demaurex, and P. Cosson. 2009. From the Cover: STIM1-induced precortical and cortical subdomains of the endoplasmic reticulum. *Proc Natl Acad Sci U S A*. 106:19358-19362.

Phillips, M.J., M. Oda, V.D. Edwards, G.R. Greenberg, and K.N. Jeejeebhoy. 1974. Ultrastructural and functional studies of cultured hepatocytes. *Lab Invest*. 31:533-542.

Phillips, M.J., M. Oda, E. Mak, V. Edwards, I. Yousef, and M.M. Fisher. 1976. The bile canalicular network in vitro. *J Ultrastruct Res*. 57:163-167.

Porter, K.R., and G.E. Palade. 1957. Studies on the endoplasmic reticulum. III. Its form and distribution in striated muscle cells. *J Biophys Biochem Cytol*. 3:269-300.

Raychaudhuri, S., and W.A. Prinz. 2010. The diverse functions of oxysterol-binding proteins. *Annu Rev Cell Dev Biol*. 26:157-177.

Roman-Fernandez, A., J. Roignot, E. Sandilands, M. Nacke, M.A. Mansour, L. McGarry, E. Shanks, K.E. Mostov, and D.M. Bryant. 2018. The phospholipid PI(3,4)P2 is an apical identity determinant. *Nat Commun*. 9:5041.

Rosenbluth, J. 1962. Subsurface cisterns and their relationship to the neuronal plasma membrane. *J Cell Biol*. 13:405-421.

Saheki, Y., X. Bian, C.M. Schauder, Y. Sawaki, M.A. Surma, C. Klose, F. Pincet, K.M. Reinisch, and P. De Camilli. 2016. Control of plasma membrane lipid homeostasis by the extended synaptotagmins. *Nat Cell Biol*. 18:504-515.

Schindelin, J., I. Arganda-Carreras, E. Frise, V. Kaynig, M. Longair, T. Pietzsch, S. Preibisch, C. Rueden, S. Saalfeld, B. Schmid, J.Y. Tinevez, D.J. White, V. Hartenstein, K. Eliceiri, P. Tomancak, and A. Cardona. 2012. Fiji: an open-source platform for biological-image analysis. *Nat Methods*. 9:676-682.

Schulze, A., K. Mills, T.S. Weiss, and S. Urban. 2012. Hepatocyte polarization is essential for the productive entry of the hepatitis B virus. *Hepatology*. 55:373-383.

Schulze, R.J., M.B. Schott, C.A. Casey, P.L. Tuma, and M.A. McNiven. 2019. The cell biology of the hepatocyte: A membrane trafficking machine. *J Cell Biol*. 218:2096-2112.

Shewan, A., D.J. Eastburn, and K. Mostov. 2011. Phosphoinositides in cell architecture. *Cold Spring Harb Perspect Biol*. 3:a004796.

Shigetomi, K., Y. Ono, T. Inai, and J. Ikenouchi. 2018. Adherens junctions influence tight junction formation via changes in membrane lipid composition. *J Cell Biol*. 217:2373-2381.

Slochower, D.R., Y.H. Wang, R.W. Tourdot, R. Radhakrishnan, and P.A. Janmey. 2014. Counterion-mediated pattern formation in membranes containing anionic lipids. *Adv Colloid Interface Sci*. 208:177-188.

Sohn, M., P. Ivanova, H.A. Brown, D.J. Toth, P. Varnai, Y.J. Kim, and T. Balla. 2016. Lenz-Majewski mutations in PTDSS1 affect phosphatidylinositol 4-phosphate metabolism at ER-PM and ER-Golgi junctions. *Proc Natl Acad Sci U S A*. 113:4314-4319.

Sohn, M., M. Korzeniowski, J.P. Zewe, R.C. Wills, G.R.V. Hammond, J. Humpolickova, L. Vrzal, D. Chalupska, V. Veverka, G.D. Fairn, E. Boura, and T. Balla. 2018. PI(4,5)P2 controls plasma membrane PI4P and PS levels via ORP5/8 recruitment to ER-PM contact sites. *J Cell Biol*. 217:1797-1813.

Stefan, C.J. 2020. Endoplasmic reticulum-plasma membrane contacts: Principals of phosphoinositide and calcium signaling. *Curr Opin Cell Biol*. 63:125-134.

Sun, E.W., A. Guillen-Samander, X. Bian, Y. Wu, Y. Cai, M. Messa, and P. De Camilli. 2019. Lipid transporter TMEM24/C2CD2L is a Ca(2+)-regulated component of ER-plasma membrane contacts in mammalian neurons. *Proc Natl Acad Sci U S A*. 116:5775-5784.

Suzuki, E., and K. Hirosawa. 1994. Immunolocalization of a Drosophila phosphatidylinositol transfer protein (rdgB) in normal and rdgA mutant photoreceptor cells with special reference to the subrhabdomeric cisternae. *J Electron Microsc (Tokyo)*. 43:183-189.

Thevenaz, P., U.E. Ruttimann, and M. Unser. 1998. A pyramid approach to subpixel registration based on intensity. *IEEE Trans Image Process*. 7:27-41.

Treyer, A., and A. Musch. 2013. Hepatocyte polarity. *Compr Physiol*. 3:243-287.

van Vliet, A.R., F. Giordano, S. Gerlo, I. Segura, S. Van Eygen, G. Molenberghs, S. Rocha, A. Houcine, R. Derua, T. Verfaillie, J. Vangindertael, H. De Keersmaecker, E. Waelkens, J. Tavernier, J. Hofkens, W. Annaert, P. Carmeliet, A. Samali, H. Mizuno, and P. Agostinis. 2017. The ER Stress Sensor PERK Coordinates ER-Plasma Membrane Contact Site Formation through Interaction with Filamin-A and F-Actin Remodeling. *Mol Cell*. 65:885-899 e886.

van Zeijl, L., B. Ponsioen, B.N. Giepmans, A. Ariaens, F.R. Postma, P. Varnai, T. Balla, N. Divecha, K. Jalink, and W.H. Moolenaar. 2007. Regulation of connexin43 gap junctional communication by phosphatidylinositol 4,5-bisphosphate. *J Cell Biol*. 177:881-891.

Vance, J.E. 1990. Phospholipid synthesis in a membrane fraction associated with mitochondria. *J Biol Chem*. 265:7248-7256.

Wang, L., and J.L. Boyer. 2004. The maintenance and generation of membrane polarity in hepatocytes. *Hepatology*. 39:892-899.

West, M., N. Zurek, A. Hoenger, and G.K. Voeltz. 2011. A 3D analysis of yeast ER structure reveals how ER domains are organized by membrane curvature. *J Cell Biol*. 193:333-346.

Willars, G.B., S.R. Nahorski, and R.A. Challiss. 1998. Differential regulation of muscarinic acetylcholine receptor-sensitive polyphosphoinositide pools and consequences for signaling in human neuroblastoma cells. *J Biol Chem*. 273:5037-5046.

Wu, Y., C. Whiteus, C.S. Xu, K.J. Hayworth, R.J. Weinberg, H.F. Hess, and P. De Camilli. 2017. Contacts between the endoplasmic reticulum and other membranes in neurons. *Proc Natl Acad Sci U S A*. 114:E4859-E4867.

Yan, D., M.I. Mayranpaa, J. Wong, J. Perttila, M. Lehto, M. Jauhiainen, P.T. Kovanen, C. Ehnholm, A.J. Brown, and V.M. Olkkonen. 2008. OSBP-related protein 8 (ORP8) suppresses ABCA1 expression and cholesterol efflux from macrophages. *J Biol Chem*. 283:332-340.

Zimmer, S.E., and A.P. Kowalczyk. 2020. The desmosome as a model for lipid raft driven membrane domain organization. *Biochim Biophys Acta Biomembr*. 1862:183329.

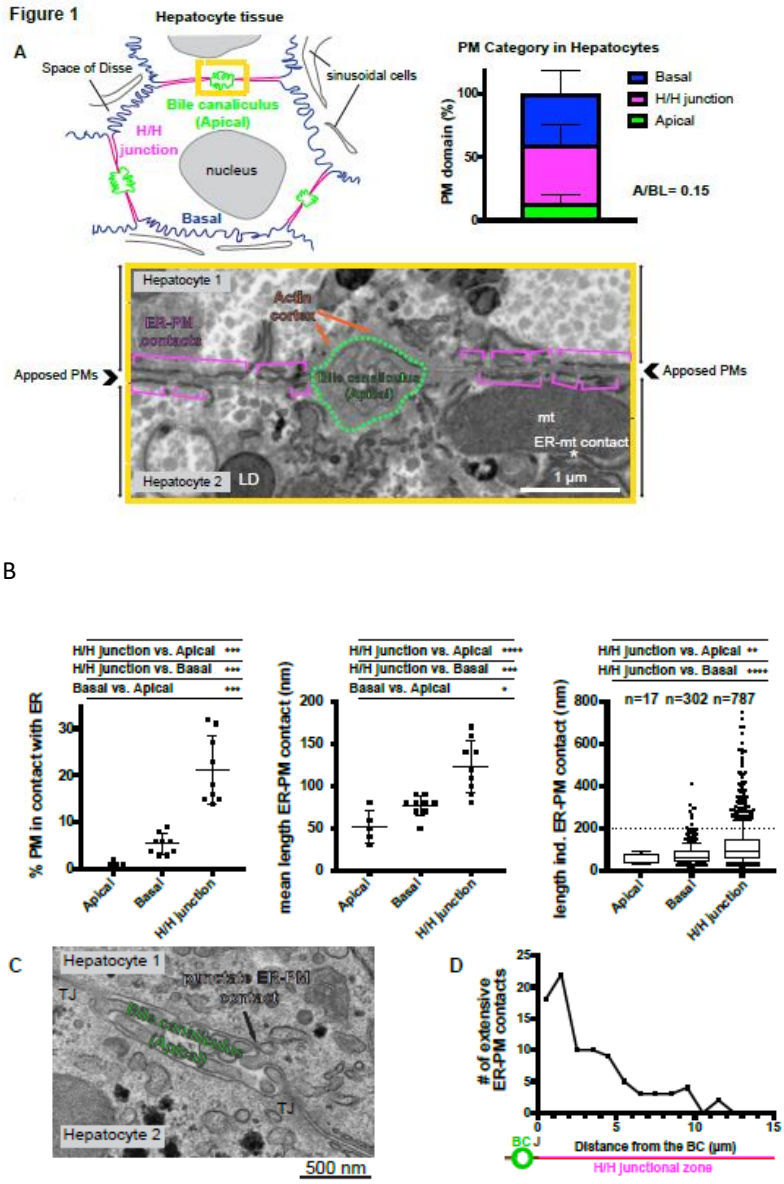

Figure 1. The quantity and length of ER-PM contacts in hepatocytes are PM domain-specific.

(A) An annotated diagram of hepatocyte tissue. The apical PM domains that form bile canaliculi (BC), lateral domains that form hepatocyte-hepatocyte cell junctions (H/H junction), and basal PM domains are coloured in green, magenta and blue respectively. The bar chart displays the proportion of each PM domain (mean % of perimeter ± SD), derived from EM analyses of 9 hepatocytes from 3 animals (see Figure S1A for the workflow). The EM image is a representative example of the apical domain and junctional zone in two

apposed hepatocytes (yellow box). The dashed green line marks the BC formed by the apposed apical domains; the magenta brackets indicate the ER-PM contacts in the lateral domains (H/H junction). mt: mitochondria; LD: lipid droplet; asterisk (*): ER-mitochondria contact. (B) Quantitative analyses of ER-PM contacts in hepatocytes. The scatter dot plots show the percentage of the PM in contact with the ER (left panel) and the average length of ER-PM contacts (middle panel) in different PM domains. Data are mean ± SD analyzed by one-way ANOVA (Tukey's multiple comparison test: ****$p<0.0001$; ***$p<0.001$; **$p<0.01$; *$p<0.1$). The box and whisker plot (right panel) depicts the median length and 10–90 percentiles of individual ER-PM contacts in the different PM domains of hepatocytes. We defined ER-PM contacts with length >200 nm as "extensive ER-PM contacts". (C) An example of a punctate ER-PM contact (black arrow) in the apical domain is shown. (D) The frequency distribution of extensive ER-PM contacts from the boundary of the BC (0 μm; defined by the end of the apical boundary formed by the tight junction, J) to the distal end of the lateral domain (H/H junctional zone) up to 15 μm. Data summarise distribution of the extensive ER-PM contacts from both sides of the BC (n = 22 cells).

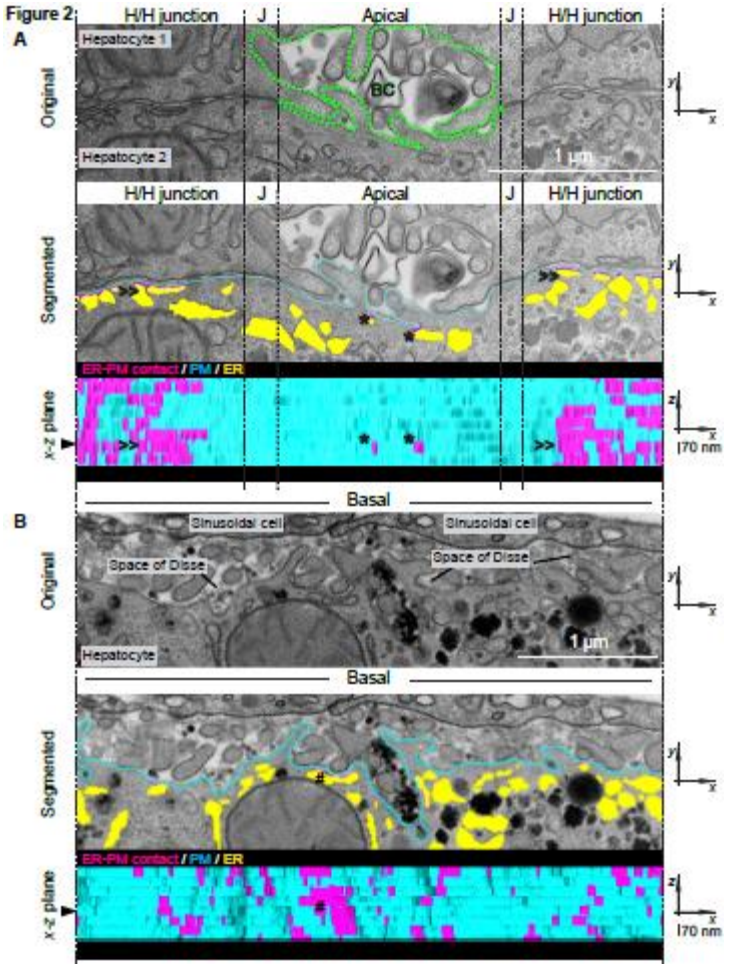

Figure 2. Segmentation analysis of ER-PM contacts in EM serial sections reveals distinct morphologies in different PM domains.

The PM, ER, and ER-PM contacts in **(A)** the apical domain and lateral domain (H/H junction) and **(B)** the basal domain of hepatocytes were analyzed by EM serial sectioning, tracing, and 3D reconstruction. The top panel in (A) is a labelled electron micrograph of two apposed hepatocytes depicting the apical and lateral (H/H junction) domains; the tight junctions that defined the apical boundary are also indicated (J). The green dashed line marks the region of the BC. The top panel in (B) shows the basal domain facing the sinusoidal cells and the Space of Disse. The middle panels (A and B) display the traces of the PM (cyan), ER (yellow) and ER-PM contacts (magenta) on the electron micrographs shown in the top panels by manual segmentation. The segmented membranes and ER-PM contacts from 8 continuous slices (70 nm thick per slice) were reconstructed to 3D models. Their ultrastructure in the

different PM domains can be visualised in Videos 1 and 2. The bottom panels (A and B) display the 3D model aligned to *x*-*z* axes with the intracellular side facing the observer, showing only the PM (cyan) and the tethering of the ER-PM contacts (magenta). The black arrowhead indicates the position of the segmented slice (middle panel) within the 3D model, vertical scale bar = 70 nm. Asterisk (*), chevrons (>>), and hashtag (#) annotate the examples of ER-PM contacts that possess distinctive morphology in the corresponding PM domains.

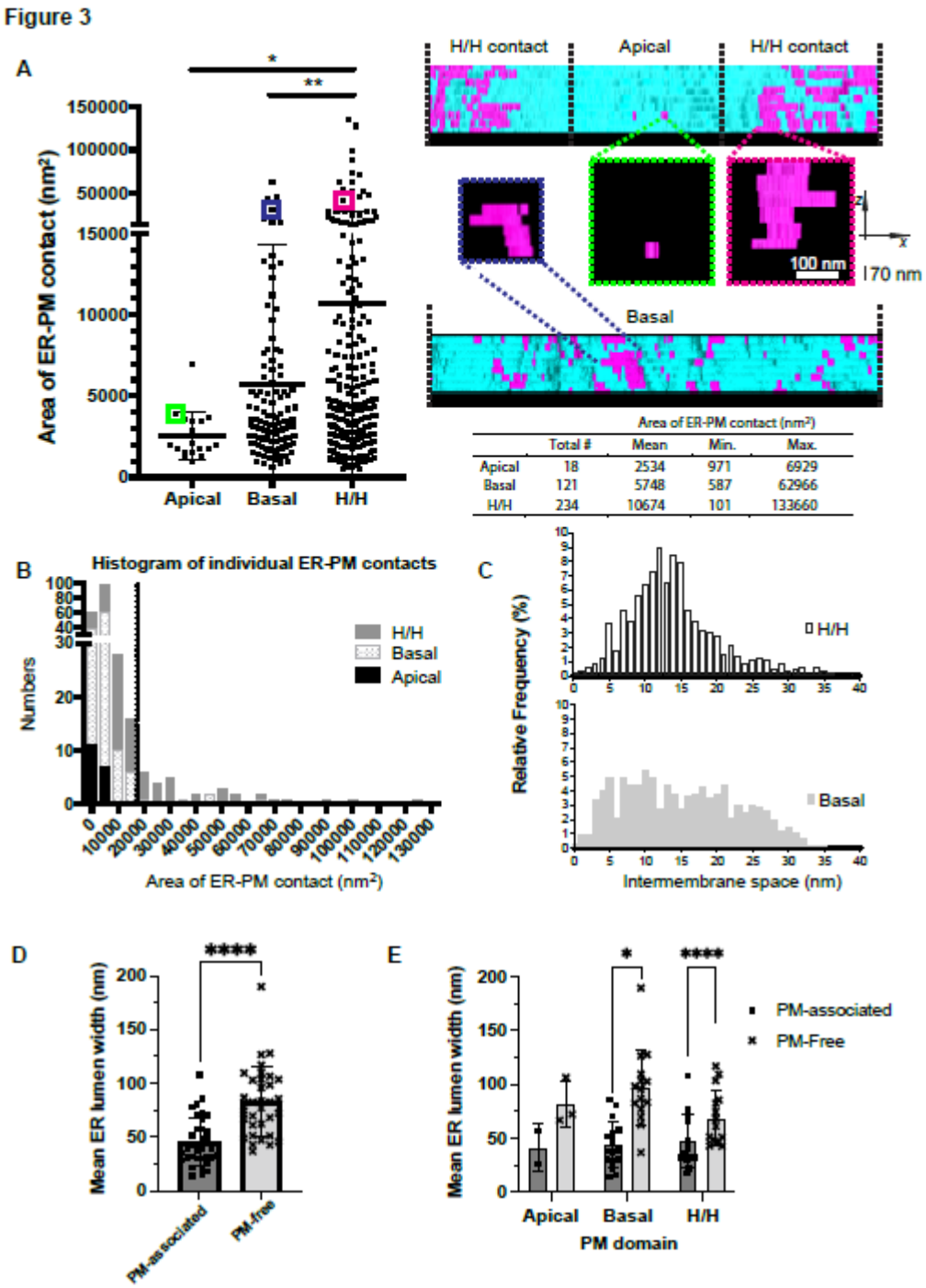

Figure 3. Quantitative analyses of the physical features of ER-PM contacts at different PM domains.

(A) The scatter dot plot shows the area of the ER-PM contacts (mean ± SD) derived from the *x*-z projections of the reconstructed 3D models (apical domain and lateral domain that forms inter-cellular junctions between hepatocytes (H/H junction) N = 3; basal domain N = 2 ; approximately equal numbers of voxels per PM domain were compared). Data were analyzed

by one-way ANOVA followed by a Tukey's multiple comparison test: **p<0.01; *p<0.1. Panels on the right serve as a visual comparison of the largest ER-PM contact in each PM domain from Figure 2. The area of the selected ER-PM contacts is indicated by the coloured boxes in the plot. The table summarises the descriptive statistics of the scatter plot. (B) Histogram reveals the area distribution of ER-PM contacts in each PM domain. (C) Histograms show the relative frequency of intermembrane space of the ER-PM contacts in the lateral (H/H junction) and basal domain, with a bin width of 1 nm. Number of ER-PM contacts analyzed: H/H junction n = 27, basal domain n = 24. (D and E) The ER lumen width (mean ± SD) of PM-associated ER and PM-free ER in all PM domains and different PM domains respectively, data were analyzed by two-tailed t-test: ****p<0.001; *p<0.05. Number of ER structures analyzed: PM-associated ER n = 34, PM-free ER n = 33.

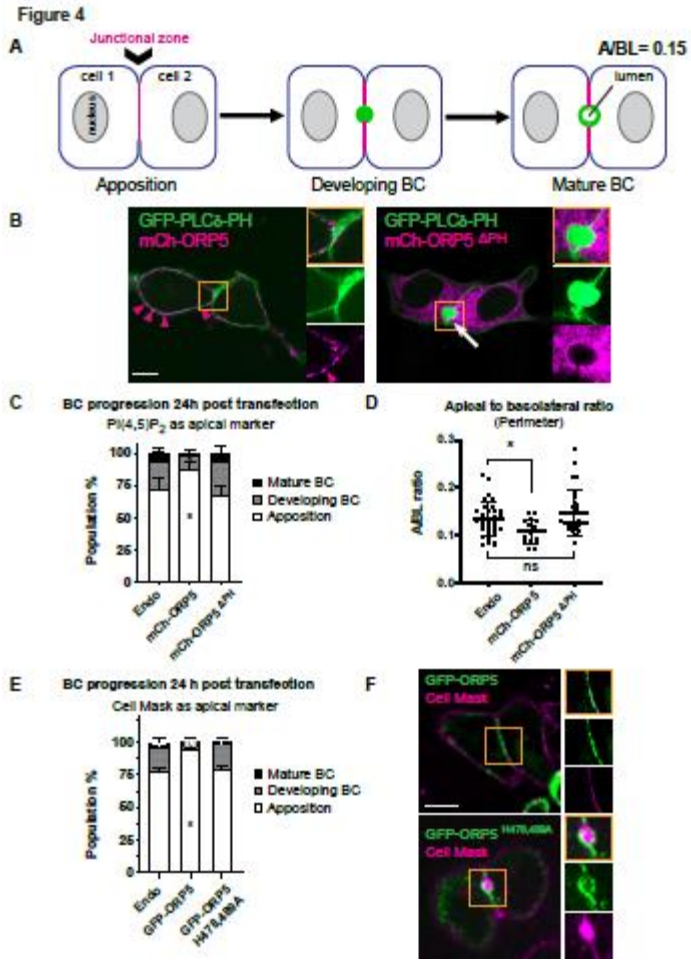

Figure 4. Overexpression of ORP5 impairs BC development and decreases apical to basolateral aspect ratio.

(A) A cartoon illustrates BC development in hepatocyte cell lines and the morphological characters associated with each stage. The basal PM, lateral PM (that forms cell-cell junctions), and apical PM (that forms the BC) are coloured in blue, magenta and green respectively. (B) Confocal microscopy images of live HepG2 couplets co-transfected with a $PI(4,5)P_2$ reporter as a PM marker (green) and mCherry-tagged ORP5 variant (magenta). Inset: 2X magnification of the apposed region (orange box) in each cell couplet. Magenta arrowheads indicate WT ORP5 localization at the PM. White arrows indicate the developing BC. Scale bar = 10 μm. (C) Number of the transfected HepG2 couplets at each BC developmental stage (mean % ± SD); N = 4 independent experiments. Data were analyzed by one-way ANOVA followed by Dunnett's test: *$p<0.05$; control column: Endo. Number of

cell couplets analyzed: Endo n = 96, mCh-ORP5 n = 79, mCh-ORP5 ΔPH n =89. (D) The apical to basolateral (A/BL) PM ratio in mature HepG2 couplets expressing the ORP5 variants and a $PI(4,5)P_2$ reporter as a PM marker. Data are shown as mean ± SD and were analyzed by one-way ANOVA (Dunnett's test: *$p<0.1$; N = 3 independent experiments; n ≅ 30 cell couplets per condition). (E) Number of HepG2 couplets at each developmental stage (mean % ± SD); cell couplets were transfected with GFP-tagged ORP5 variants and labelled with CellMask PM dye. Results follow the identical statistical analysis described in (C). Number of cell couplets analyzed: Endo n = 88, GFP-ORP5 n = 70, GFP-ORP5 H478,479A n = 75; **$p<0.001$, *$p<0.1$; N = 3 independent experiments. (F) Live images of HepG2 couplets transfected with GFP-tagged ORP5 variants (green) and labelled with CellMask (magenta). Inset: 2X magnification of the apposed region (orange box) in each cell couplet. Scale bar = 10 μm.

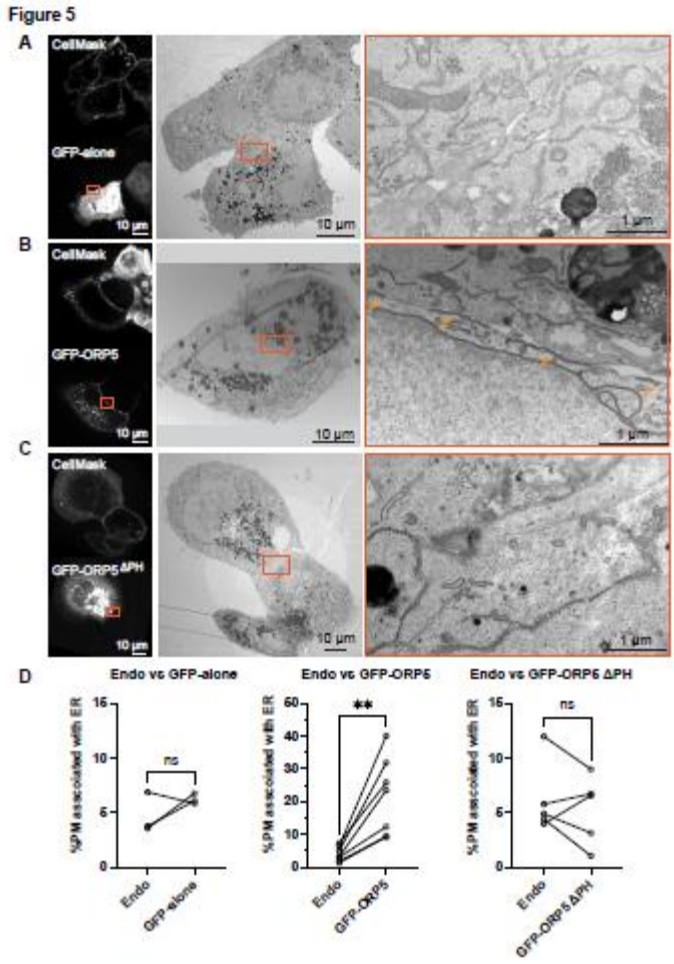

Figure 5. ORP5 modulates ER-PM contacts at sites of cell-cell adhesion.

CLEM analyses of HepG2 couplets where only one cell within the couplet expressed (A) GFP-alone (B) GFP-ORP5 or (C) GFP-ORP5 ΔPH. The cell couplets are at the cell-cell apposition stage and are labelled with CellMask. Dotted boxes at low magnification annotate the corresponding region of interest shown in the high magnification images. Orange arrows in panel B indicate the presence of extensive ER-PM contacts at the lateral PM of the GFP-ORP5 transfected cell within the couplet. Scale bar, as indicated. (D) Linked dot plots summarize the impact of GFP, GFP-ORP5, or GFP-ORP5 ΔPH overexpression on ER-PM contact formation at sites of cell-cell apposition. Number of half-transfected couplets analyzed: GFP-alone n = 3, GFP-ORP5 n = 7, GFP-ORP ΔPH PH n=5. Data were analyzed by paired t-test: **p<0.01.

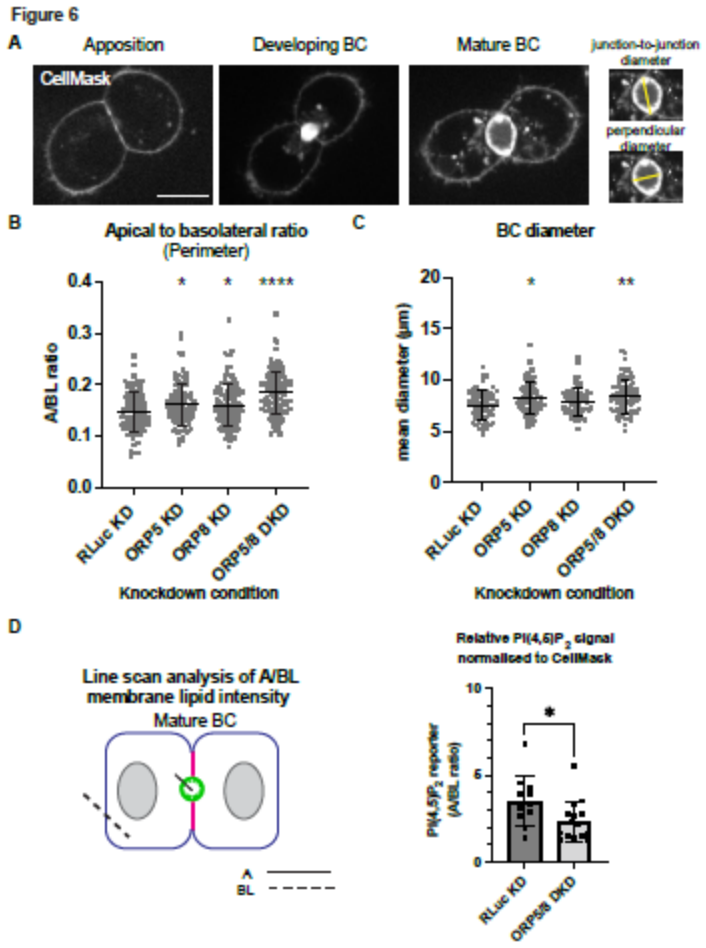

Figure 6. Depletion of ORP5 and ORP8 increases apical to basolateral aspect ratio.

(A) HepG2 cell couplets stained with CellMask PM dye at different developmental stages. Scale bar = 10 µm. (B) Apical to basolateral ratio (A/BL) and (C) BC diameter of mature HepG2 couplets upon siRNA-mediated depletion of ORP5 and ORP8. The BC diameter is the average value of the junction-to-junction diameter and the perpendicular diameter. siRNA targeting *Renilla* Luciferase (RLuc) was used as the control condition. Data are displayed as mean ± SD and were analyzed by one-way ANOVA (Dunnett's test: *p<0.1, **p<0.01,****p<0.0001; n ≅ 100 couplets per condition for A/BL ratio and n ≅ 60 couplets per condition for mean diameter). N = 3 independent experiments. (D) The diagram illustrates the line scan approach used to measure the apical to basolateral lipid intensity of mature HepG2 couplets. (E) Spatial ratiometric fluorescence analysis of the PI(4,5)P_2 reporter normalized to CellMask signals (as an indicator of total membrane content) in control and ORP5/8 depleted HepG2 couplets. The plots display the normalized apical to basolateral (A/BL) PI(4,5)P_2 reporter intensity (mean ± SD) in mature HepG2 couplets. Data were analyzed by two-tailed t-test *p<0.05; n ≅ 15 cell couplets.

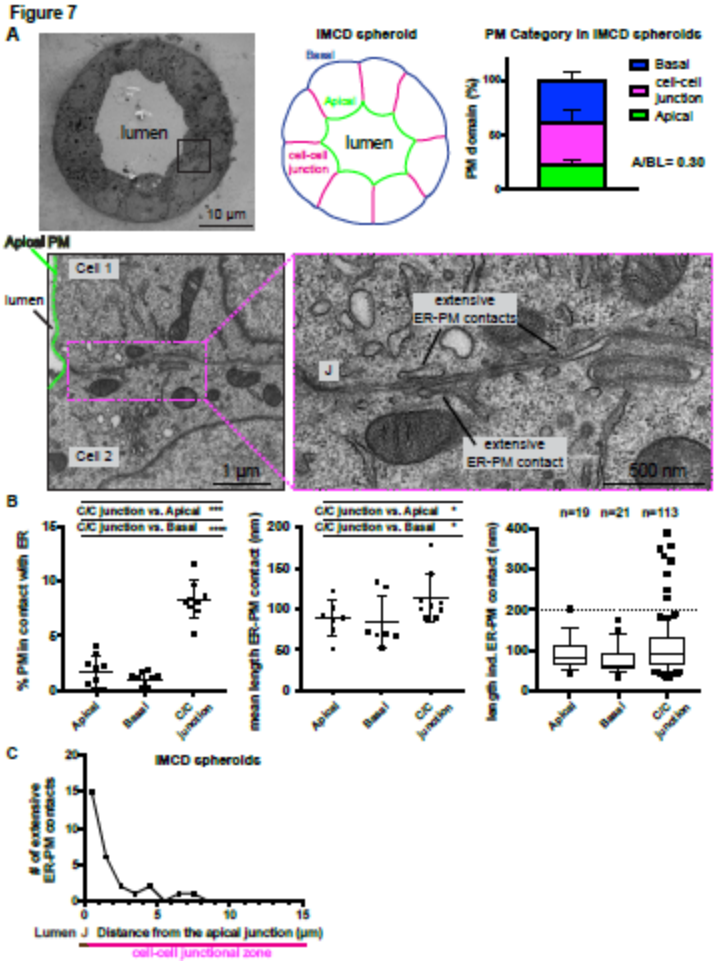

Figure 7. The PM domain-specific distribution of ER-PM contacts is conserved in IMCD spheroids.

(A) An electron micrograph showing a cross-section of an entire IMCD spheroid and a colour-coded diagram depicting different PM domains within the spheroid (apical = green; basal = blue; cell-cell junction = magenta). The bar chart displays the proportion of each PM domain by perimeter (mean ± SD) in polarized IMCD cells, summarizing EM analyses of 9 cells from 3 spheroids. The magnified electron micrographs highlight two apposed cells within the spheroid (black dashed box); apical PM is outlined in green and the extensive ER-PM contacts (length > 200 nm) are annotated in the highest magnification. J: cell junction. (B) Quantitative analyses of ER-PM contacts in IMCD spheroids, identical to the analyses described in Figure 1B. Data of the scatter dot plots were analyzed by one-way ANOVA followed by a Tukey's multiple comparison test: ****p<0.0001; ***p<0.001; *p<0.1. (C) The frequency distribution of extensive ER-PM contacts from the boundary of the lumen (0 µm = cell junction) to the distal end of the lateral domain up to 15 µm, data gathered from n = 41 cells.

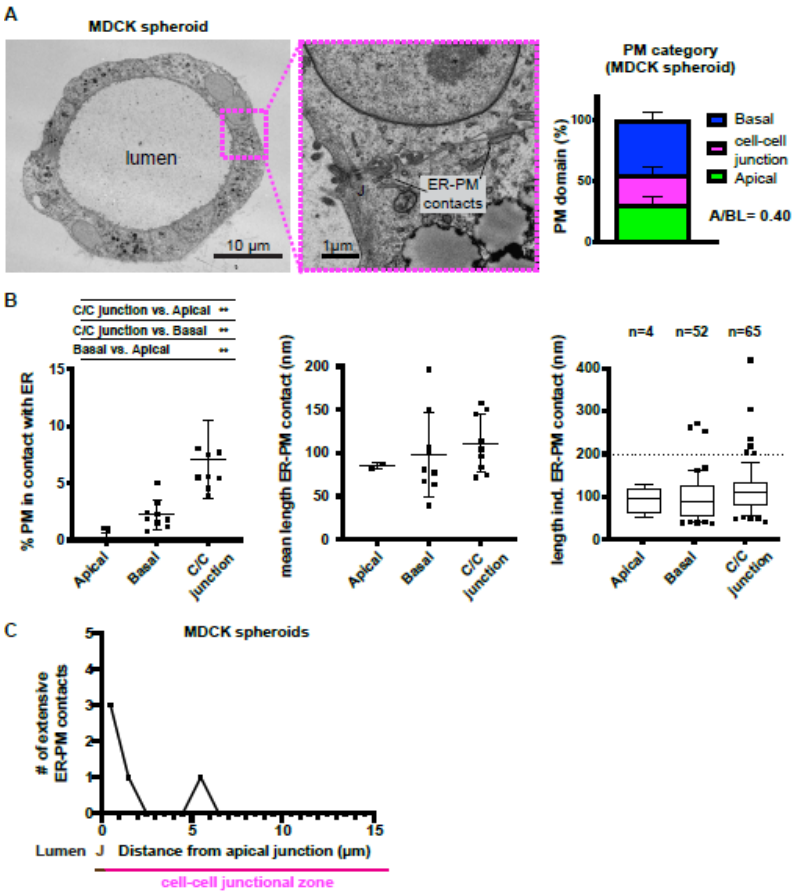

Figure 8. The PM domain-specific distribution of ER-PM contacts is conserved in MDCK spheroids.

(A) An Electron micrograph showing a cross-section of an entire MDCK spheroid. The magnified electron micrograph highlights two apposed cells within the spheroid and the location of the ER-PM contacts (magenta dashed box; J: cell junction). The bar chart displays the proportion of each PM domain by perimeter (mean ± SD) in polarized MDCK cells, summarising EM analyses of 9 cells from 3 spheroids. (B) Quantitative analyses of ER-PM contacts in MDCK spheroids, identical to the analyses described in Figure 1B. Data of the scatter dot plots were analyzed by one-way ANOVA followed by a Tukey's multiple comparison test: **p<0.005. (C) The frequency distribution of extensive ER-PM contacts from the boundary of the lumen (0 µm = cell junction) to the distal end of the lateral domain up to 15 µm, data gathered from n = 9 cells.